Microfluidic Mixing and the Formation of Nanoscale Lipid Vesicles

Andreas Jahn,*,†,§,⊥ Samuel M. Stavis,†,⊥ Jennifer S. Hong,† Wyatt N. Vreeland,‡ Don L. DeVoe,§ and Michael Gaitan†

†National Institute of Standards and Technology, Semiconductor Electronics Division, Gaithersburg, Maryland 20899, ‡National Institute of Standards and Technology, Biochemical Science Division, Gaithersburg, Maryland 20899, and §University of Maryland, Mechanical Engineering Department, College Park Maryland 20742. ⊥The first and second authors contributed equally to this publication.

ABSTRACT We investigate the formation of unilamellar lipid vesicles (liposomes) with diameters of tens of nanometers by controlled microfluidic mixing and nanoparticle determination (COMMAND). Our study includes liposome synthesis experiments and numerical modeling of our microfluidic implementation of the batch solvent injection method. We consider microfluidic liposome formation from the perspective of fluid interfaces and convective-diffusive mixing, as we find that bulk fluid flow parameters including hydrodynamically focused alcohol stream width, final alcohol concentration, and shear stress do not primarily determine the vesicle formation process. Microfluidic device geometry in conjunction with hydrodynamic flow focusing strongly influences vesicle size distributions, providing a coarse method to control liposome size, while total flow rate allows fine-tuning the vesicle size in certain focusing regimes. Although microfluidic liposome synthesis is relatively simple to implement experimentally, numerical simulations of the mixing process reveal a complex system of fluid flow and mass transfer determining the formation of nonequilibrium vesicles. These results expand our understanding of the microfluidic environment that controls liposome self-assembly and yield several technological advances for the on-chip synthesis of nanoscale lipid vesicles.

KEYWORDS: liposome · lipid vesicle · nanoparticle · microfluidic mixing · hydrodynamic focusing · microfluidic injection · simulation

Liposomes were first described in 1965 by Bangham *et al.*, when the exposure of phospholipid films to excess water gave rise to the formation of lamellar structures that were able to sequester aqueous solutions.[1] The ability to encapsulate compounds drove initial applications of lipid vesicles as drug delivery vehicles, but early liposome formulations had limited commercial success because of colloidal and biological instability.[2] Further widespread application of liposomes as artificial drug carriers has been hindered by limited reproducibility of particle size, high cost of creating custom formulations, and indeterminate stability.[3]

Our liposome formation technique, controlled microfluidic mixing and nanoparticle determination (COMMAND), addresses several of these issues. COMMAND utilizes microfluidic hydrodynamic focusing to precisely control the convective-diffusive mixing of miscible liquids under laminar flow and determine the self-assembly of phospholipid molecules into nanoscale liposomes.[4−7] This enables the controlled formation of liposomes ranging in mean diameter from about 50−150 nm with relative standard deviations ranging from <10% for smaller vesicle distributions to <20% for larger vesicle distributions. COMMAND compares favorably in this regard to many other techniques for the preparation of nanoscale liposomes, although direct and quantitative comparisons of liposome size are complicated by the use of different characterization techniques (*e.g.*, dynamic light scattering with or without prior size fractionation, freeze fracture electron microscopy, cryogenic transmission electron microscopy). For example, a modified thin-film hydration method has been used to synthesize liposomes with diameters dispersed from 170 to 230 nm.[8] Detergent dialysis has been used to synthesize liposomes dispersed from 15 to 150 nm.[9] Inkjet printing was used to synthesize liposomes dispersed from 50 to 200 nm.[10] A dense gas technique involving depressurization of expanded solution into aqueous media has been used to synthesize liposomes dispersed from 50 to 200 nm.[8] A rapid extrusion procedure utilizing stacked polycarbonate filters with pore sizes ranging from 30 to 400 nm produced liposomes with a dispersity of >25% (relative standard deviation).[11] Freeze-drying of a monophase solution was used to produce liposomes dispersed from 100 to 200 nm, and an industrial scale ethanol injection technique was used to synthesize liposomes dispersed from 50 to 400 nm.[12,13] Liposomes with diameters at the smaller end of the 50 to 150 nm size range are important for drug

*Address correspondence to andreas.jahn@org.chem.ethz.ch.

Received for review April 29, 2009 and accepted March 22, 2010.

Published online March 31, 2010. 10.1021/nn901676x

delivery and gene therapy applications because of reduced opsonization in the bloodstream.[14,15] Liposomes at the larger end of this size range are useful as engineered nanostructures for a variety of other applications, including as templates for nanoparticle formation,[16−18] as carriers of many markers to provide immunoassay signal amplification,[19] and as nanoscale vials for molecular encapsulation and confinement.[20] Microfluidic hydrodynamic focusing has subsequently been applied to the directed self-assembly of other amphiphilic particles and block copolymers,[21] as well as to the self-assembly of mesoscale spherical quantum dot compound micelles.[22]

Additional advantages of COMMAND include the elimination of size homogenization postprocessing procedures (defined here as procedures that subject previously formed liposomes to external forces in order to rupture the bilayer membrane) such as membrane extrusion and sonication and the ability to control vesicle size reproducibly.[23−25] Other methods such as dialysis and dilution allow the direct formation of liposome formulations but are often limited by poor reproducibility or time-consuming synthesis processes.[26] The elimination of postprocessing to homogenize vesicle size is an important benefit that is congruent with the demands of personalized medicine applications such as drug delivery and gene therapy, which require reproducible vesicle size distribution and consistency from batch to batch. Such applications also drive the need for real-time liposome synthesis processes compatible with lab-on-a-chip technologies. On-chip integration of liposome synthesis would facilitate the multiplexed delivery of nanoscale vesicles to target cells for the high throughput discovery and screening of therapeutic agents, as well as point-of-care personalized liposome therapeutic treatment. An integrated and mobile microfluidic platform could also minimize lipid oxidation and hydrolysis, which are known to reduce liposome stability and limit applications thereof.

Despite the longstanding interest in liposome applications and the growing interest in microfluidic approaches to the synthesis of nanoscale lipid vesicles (and other types of nanoparticles),[4] a fundamental understanding of the lipid-to-liposome self-assembly mechanism has remained limited, in part by current methods of liposome formation and characterization. In many conventional nanoscale liposome synthesis techniques, vesicle formation is primarily determined by macroscopic experimental parameters such as injection flow velocity, injection pressure, or stirring rate. The ability to precisely control and characterize microscopic mixing conditions and the associated impact on vesicle formation is limited by the chaotic nature of mixing under the turbulent conditions associated with "batch" processing or obscured by the visual inaccessibility of mixing dynamics.[13,27,28] Another recent microfluidic approach to synthesize nanoscale vesicles is based on relatively complex mixing dynamics.[10]

In contrast to the batch solvent injection method from which it is adapted, COMMAND enables precise steady-state control over the mixing of miscible liquids under laminar flow conditions.[27,28] This results in predictable and repeatable mixing across microfluidic interfaces and the continuous synthesis of liposome size distributions of controlled size. Under laminar fluid flow, the mixing of miscible liquids is governed by molecular diffusion as influenced by convection, which facilitates numerical simulation of the alcohol−water interface. Relevant simulations include concentration profiles of alcohol−water mixtures for different hydrodynamic focusing conditions, total flow rate, and viscous anisotropy which is often inherent to miscible solvent−water combinations.[29−32] These various attributes enable the controlled investigation of vesicle formation, and, because COMMAND is accessible with optical microscopy, observed and simulated microfluidic environments can be compared and validated. These attributes also differentiate COMMAND from a variety of other microfluidic approaches to the formation of microscale and nanoscale droplets, vesicles, and tubules. COMMAND exploits the steady-state convective-diffusive mixing of miscible liquids to control microfluidic environmental polarity and direct the self-assembly of amphiphilic molecules into kinetically trapped nanometer scale vesicles. This approach is fundamentally different from a growing number of microfluidic techniques that utilize mechanical shear forces and capillary instability between immiscible liquids to form vesicles or droplets stabilized by surfactants,[33,34] or techniques that apply mechanical forces to lipid bodies to form microscale lipid vesicles or microscale and nanoscale lipid tubules.[35−38] The on-chip format of COMMAND also distinguishes it from other novel microfluidic approaches to nanoscale vesicle synthesis which are not as conducive to the investigation of the lipid-to-liposome self-assembly process.[10]

In this manuscript, we present a detailed study of deterministic liposome formation by controlled microfluidic mixing. We performed liposome synthesis experiments to investigate the dependence of liposome size distribution on microfluidic device geometry, hydrodynamic flow focusing, and volumetric flow rate. Our experimental results show that liposome size distributions are not only a function of flow rate ratio (FRR), as previously hypothesized,[5,6] but also a function of device size and scaling, and total flow rate, and we discuss the technological consequences of these findings. We then use numerical simulations of the convective-diffusive mixing of isopropyl alcohol (IPA) and water to relate the results of our synthesis experiments and correlate liposome size with microfluidic mixing conditions. We interpret this correlation through a critical mixing time which kinetically limits the growth and coa-

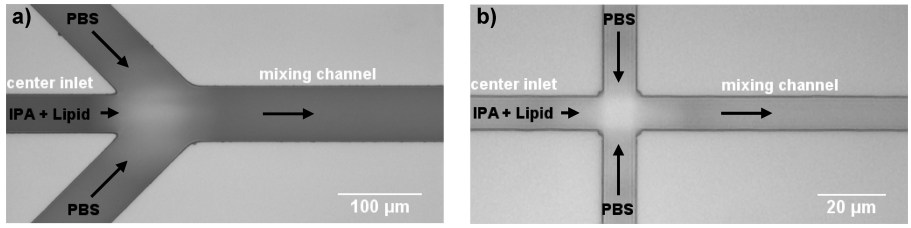

Figure 1. Optical micrographs of microfluidic devices used for liposome synthesis with COMMAND. Microchannels were etched in silicon substrates and sealed with borosilicate glass cover wafers *via* anodic bonding. (a) All channels are 120 μm deep, the left center inlet channel is 42 μm wide, and the oblique side channels are 65 μm wide. The mixing channel is 65 μm wide and 10 mm long. (b) All channels are 36 μm deep and 10 μm wide. The mixing channel is 10 mm long. Arrows indicate the direction of fluid flow.

lescence of intermediate lipid fragments or micelles—an existing theory for the mechanism of nonequilibrium lipid vesicle formation—and we discuss the implications of our work for future investigations of the microfluidic directed self-assembly of nanoscale vesicles.

RESULTS AND DISCUSSION

The primary motivation for our work is to investigate the formation of kinetically trapped lipid vesicles ranging in diameter from 50 to 150 nm, as determined by microfluidic mixing. In contrast to equilibrium structures such as micelles, which tend to rapidly exchange surfactants and contents, kinetically trapped lipid vesicles are more stable and maintain size, structure, and desirable chemical properties for extended times after administration.[19] As a result, kinetically trapped nanoscale lipid vesicles facilitate the application of liposomes as drug carriers and have important implications for other applications of liposomes as engineered nanostructures. We envision that the results of our study are not necessarily limited in scope to lipid molecules and could help to provide insight into the microfluidic directed self-assembly processes of a variety of related amphiphilic molecules of biological or synthetic origin.

Effects of Microfluidic Device Design and Hydrodynamic Flow Focusing on Liposome Size. We used two microfluidic devices to characterize the combined effects of device geometry and hydrodynamic flow focusing on liposome synthesis. The devices were well separated in design parameter space, having different channel dimensions and geometrical scaling, as shown in Figure 1.

Figure 2 shows the geometric radius (R_g) distributions for liposomes produced using a variety of hydrodynamic focusing conditions in microfluidic devices with 10 μm (Figure 2a) and 65 μm mixing channel widths (Figure 2b) at a constant total average flow velocity of 0.25 m/s. As shown in Figure 2c, the two different devices were used to synthesize similar liposome size distributions with values of R_g ranging from a peak vesicle number fraction of ~25 to ~73 nm with decreasing FRRs.

Similar liposome size distributions were obtained under different hydrodynamic flow focusing conditions and bulk fluid flow parameters. The 10 μm channel geometry produced comparable peak vesicle number fractions at approximately half the FRR and double the final alcohol concentration of the 65 μm channel geometry. Neglecting a slightly flattened parabolic flow profile in the channel due to a higher viscosity of IPA compared to PBS, the focused stream width scales linearly with the mixing channel width,[39] so that the focused stream width is approximately 6.5 times wider in the 65 μm channel than in the 10 μm channel at a given FRR. As shown in Figure 2c, the vesicle size distributions vary significantly for the same focused stream width in the 10 and 65 μm wide outlet channel devices. Figure 2c also shows that the vesicle size differs for the same FRRs, that is, equal concentrations of IPA in the sample.

These results demonstrate the difficulty in considering COMMAND from the perspective of bulk fluid flow parameters. As implemented, liposome formation is solely dependent neither on the final solvent concentration in the sample (equal FRRs in the two microchannel geometries) nor on the focused stream width (equal focused stream width in both microchannel geometries) (Figure 2c). Previous reports on bulk injection methods have suggested a higher liposome polydispersity as the solvent concentration increases,[28] but this is only partially true for liposome synthesis with COMMAND. While alcohol concentration and polarity of the fluidic environment are critical to the liposome self-assembly process, these parameters must be considered from the perspective of the IPA/PBS interface and the resulting microfluidic mixing process. Additionally, the fact that liposomes of a particular size distribution can exist at different final IPA concentrations indicates that, once formed at the IPA/PBS interface, liposomes are stable at different IPA concentrations within the vesicle size range investigated.

The similar liposome size distributions produced with different microfluidic devices also show that, within a broad range, microfluidic device size and geometry are not fundamental to COMMAND but have important technological consequences. At the onset, larger microfluidic devices are easier to fabricate and operate, and produce higher volumetric throughput with lower vesicle concentration. Device size can be in-

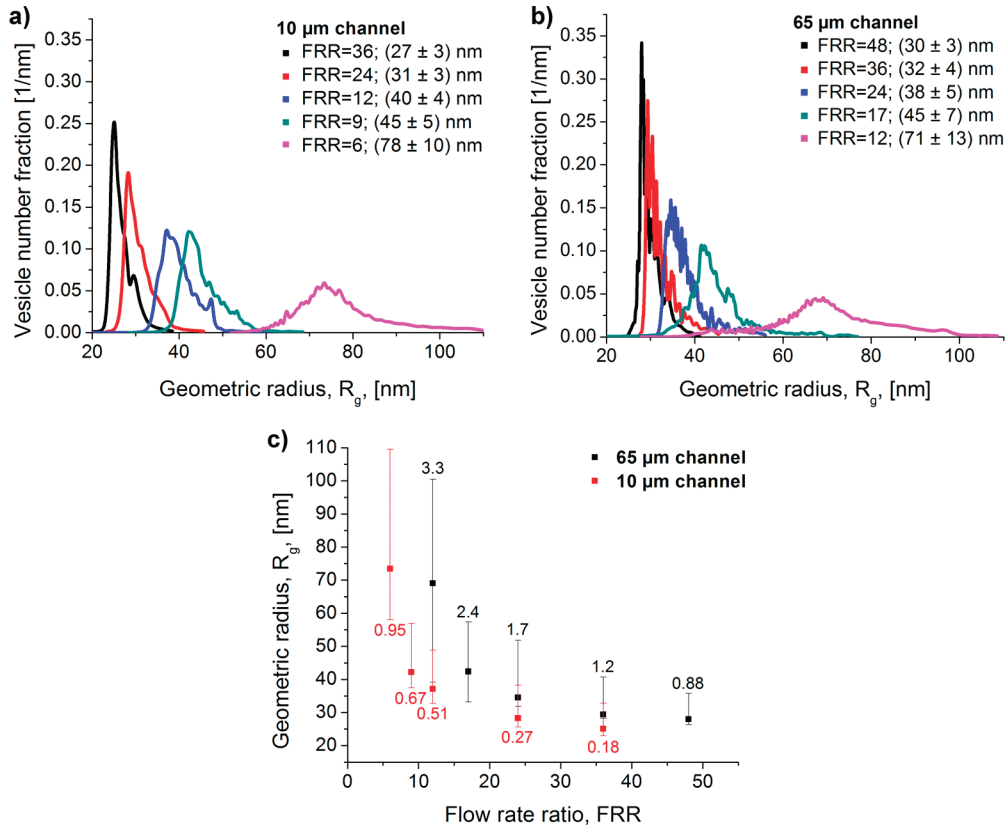

Figure 2. Dependence of liposome size on microfluidic device design and hydrodynamic flow focusing. Microfluidic device design and hydrodynamic flow focusing are shown to strongly influence the average geometric radius (R_g) of liposomes produced at different buffer-to-solvent flow rate ratios (FRRs) and constant total flow velocity v_m = 0.25 m/s. Liposome size distributions produced in the (a) 10 μm and (b) 65 μm wide channel geometry are shown (insets show average R_g ± standard deviation). (c) Liposome size distribution as a function of FRR for both channel geometries with the peak R_g value and the R_g limits at a 5% peak height. The continuum stream width in micrometers for the 10 μm (red) and 65 μm (black) wide channel geometry is shown above or below the width of the size distribution at each FRR. A decrease in FRR increases the vesicle size in both channel geometries. Comparable vesicle size distributions in the smaller channel geometry were obtained at about half the FRR of the 65 μm channel device.

creased until diffusive mixing across fluidic interfaces and into macroscopic fluidic volumes becomes prohibitively slow or turbulent mixing occurs. Smaller microfluidic devices are more difficult to fabricate and operate due to increased pressure drops and clogging issues. Smaller devices also produce lower volume throughput but with higher vesicle concentration. A higher concentration of liposomes resulting from lower focusing and increased volume fraction of lipid tincture in a smaller microchannel enables higher encapsulation efficiency for drug delivery applications. The reduced footprint of smaller microfluidic devices also allows for improved integration of COMMAND for on-chip or mobile liposome synthesis. Smaller microfluidic devices may also be capable of producing larger vesicle size distributions with lower polydispersity, as suggested by a comparison of the relative standard deviations of liposome size distributions with R_g of 45 nm and above. However, more work is required to characterize the ultimate limits of our technique in this regard.

Effects of Total Volumetric Flow Rate (Q_t) and Average Flow Velocity (v_m) on Liposome Size. We investigated the effects of volumetric flow rate (Q_t), or average fluid flow velocity (v_m), on liposome size over a wide range of hydrodynamic flow focusing conditions. Previous reports have suggested that the vesicle size distribution remains nearly unaffected by the total volumetric flow rate (Q_t).[5,6] While Q_t has little impact on average vesicle size at high focusing conditions (*i.e.*, FRR $>$ 30 in the 65 μm wide channel) (Figure 3a), its effect on R_g increased noticeably toward low focusing conditions (*i.e.*, FRR $<$ 20 in the 65 μm wide channel) (Figure 3d).

Figure 3d shows that decreasing Q_t results in smaller vesicle radii and narrower size distributions. The same trend was observed for liposome synthesis experiments performed in the smaller microfluidic device (data not shown). Figure 3d also shows that increasing Q_t changes the shape of the vesicle distribution from a skewed distribution to an increasingly symmetric distribution. A similar transition from a skewed to a more symmetric distribution was observed when decreasing the FRR (Figure 2). Figure 3d shows that a FRR of 14 at a Q_t of 25 μL/min produces a peak liposome number fraction with an R_g value of about 40 nm similar to a FRR of 19 and a Q_t of 100 μL/min (Figure 3c). This suggests that increasing Q_t beyond 100 μL/min at a FRR of 19 can

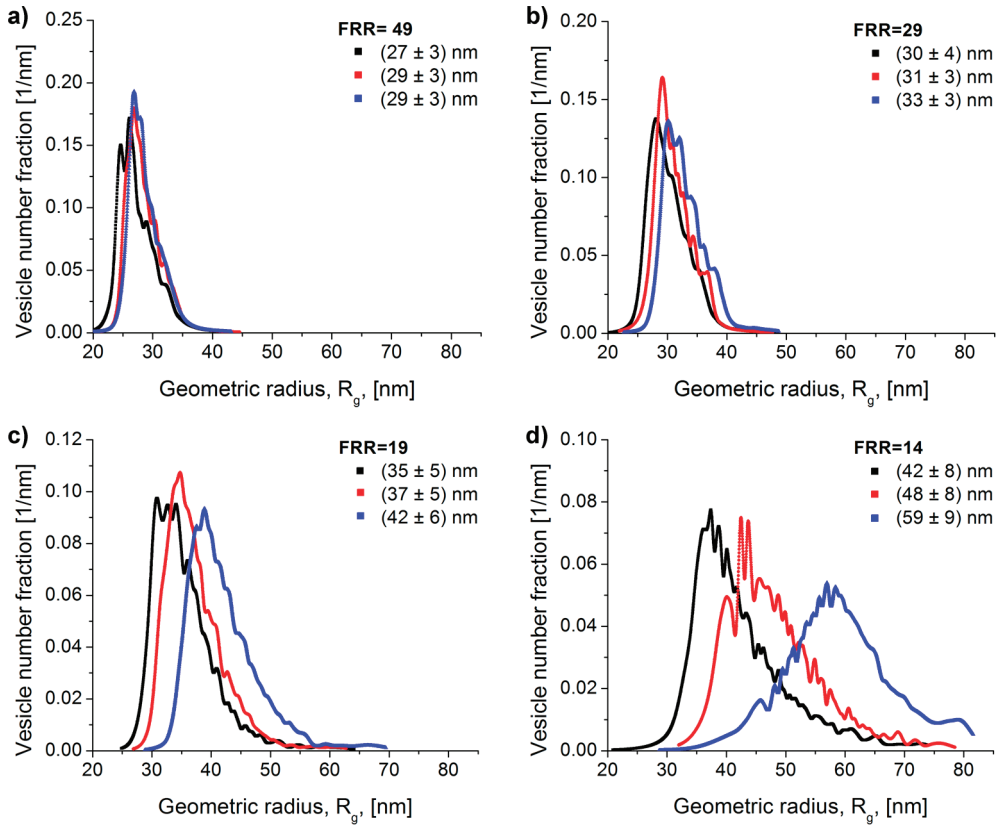

Figure 3. Dependence of liposome size on total volumetric flow rate and hydrodynamic flow focusing. For a constant FRR, the average liposome size increases with total volumetric flow rate Q_t. Plots of the measured liposome size distribution for the 65 μm wide mixing channel at three volumetric flow rates Q_t of 25 μL/min (black), 50 μL/min (red), and 100 μL/min (blue). The flow rate ratio (FRR) is held constant at (a) 49, (b) 29, (c) 19, and (d) 14 (insets show average R_g ± standard deviation). The dependence of liposome size distribution on Q_t is subtle at a high FRR of 49 and increases noticeably as the FRR decreases to 14.

produce larger and more homogeneous liposomes than are obtained at a lower FRR. Increasing Q_t has a limiting effect, however, as a more than 2-fold increase beyond 100 μL/min at low FRRs requires a longer microchannel to ensure complete mixing within the 65 μm channel device. At values of Q_t greater than 200 μL/min, bimodal liposome size distributions were obtained with very large particle diameters (data not shown) in addition to nanoscale liposomes, which suggests the formation of much larger vesicles downstream of the microchannel terminus by uncontrolled bulk mixing in the microfluidic connector and collection tube. We also observe that as FRR is increased, the vesicle radii distribution changes ever more subtly with Q_t, which provides a means for increasing synthesis throughput (Figure 3a,b) of small liposomes at high FRR. In summary, liposome formation depends on Q_t or v_m within certain focusing regimes, and Q_t can therefore be used to fine-tune the vesicle size distribution or increase liposome synthesis throughput.

Discussion of Diffusive and Convective-Diffusive Mixing Regions. COMMAND utilizes hydrodynamic focusing to precisely control microfluidic mixing and determine nanoparticle formation. In this process, a central stream is sheathed between two adjacent streams and hydrodynamically focused, which narrows the central stream to the extent that diffusive mixing occurs rapidly across its width. Micrometer-scale laminar flow, the complete miscibility between IPA and PBS, and the rapid reduction of the small viscosity difference between IPA and PBS due to diffusion result in steady state microfluidic mixing without instability along the contact interface. This makes our system suitable for numerical analysis,[39,40] and we modeled the microfluidic environments for our synthesis experiments by simulating the mixing of IPA with water. An understanding of this mixing process is essential to our investigation of liposome formation, as it is known that amphiphilic phospholipid molecules are soluble in nonpolar solvents but spontaneously self-assemble into liposomes as the polarity of the surrounding fluidic environment increases. While our hydrodynamic flow focusing system has some relevant three-dimensional characteristics, including a nonuniform velocity across the vertical plane resulting from microchannel depth to width aspect ratios of less than five and nonuniform diffusion of the focused stream across the vertical midplane due to no-slip boundary conditions at the top and bottom walls affecting the flow profile,[39,41] we approximate flow and mass transfer at the vertical midplane with two-

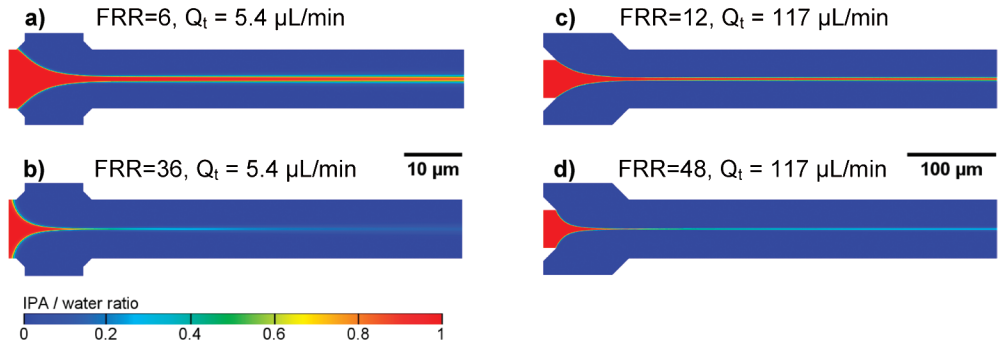

Figure 4. Numerical simulations of microfluidic device design and hydrodynamic flow focusing. Simulated IPA concentration distributions of the focused stream in the 10 μm channel geometry at a FRR of 6 (a) and 36 (b) and in the 65 μm wide channel geometry at a FRR of 12 (c) and 48 (d). The average flow velocity is 0.25 m/s in both microchannel designs and corresponds to a volumetric flow rate of Q_t = 5.4 μL/min (a, b) and Q_t = 117 μL/min (c, d) in the respective channel geometry. The simulation shows an increase in mixing and surface-to-volume ratio of the focused IPA stream in both channel geometries as the FRR increases. The IPA concentration profiles shown in the figure correspond to the highest and lowest FRR of Figure 2 of each respective geometry to reveal the substantial change in the IPA concentration distribution profile and surface-to-volume ratio.

dimensional simulations to capture the most salient features of the system for a qualitative correlation of microfluidic mixing conditions and liposome size. A recently investigated process in which a low viscosity fluid envelops a high viscosity fluid at low Peclet numbers *Pe* is not included in the simulation but is considered in further discussion.[42]

Figure 4 shows the IPA concentration profile at relatively low and high FRRs in the 10 and 65 μm channel design modeled with a constant total average flow velocity of 0.25 m/s. Low focusing, that is, FRR 6 in the 10 μm channel (Figure 4a) and 12 in the 65 μm channel (Figure 4c), results in a relatively wide center stream in which mixing time is limited by molecular diffusion in the spanwise direction (normal to streamlines).[39] This microfluidic mixing condition leads to a relatively shallow concentration gradient, a relatively low surface-to-volume ratio, and a gradual depletion of the focused center stream by mutual diffusion of the two fluids across the contact interface. Consequently, the IPA concentration remains high in the interior of the focused stream past the focusing region in the downstream diffusive mixing channel. As a result, a large fraction of lipid molecules remains solubilized and self-assembles into larger liposomes (as measured experimentally) in the downstream diffusive mixing channel, while the fraction of liposomes that forms in the convective-diffusive focusing region is low. Conversely, high focusing, that is, FRR 36 in the 10 μm channel (Figure 4b) and 48 in the 65 μm channel (Figure 4d), results in a relatively narrow center stream in which mixing time becomes dominated by two-dimensional convective−diffusive transport in the focusing region.[39] In this microfluidic mixing condition, convection abruptly reduces the width of the focused stream in the hydrodynamic focusing region, which reduces the diffusion length, enhances diffusive mixing, and results in a steep concentration gradient. High focusing (Figure 4b,d) results in a relatively high surface-to-volume ratio and the rapid depletion of the focused center stream by convective-diffusive mixing, causing more of the lipid molecules to self-assemble into smaller liposomes (as measured experimentally) within the convective−diffusive hydrodynamic focusing region. Further increases in FRR gradually change this mixing condition until a minimum mixing time is reached.[39]

Figure 5 shows the simulated concentration profiles of a focused IPA stream at a relatively low and high FRR for a low and high volumetric flow rate. Adjacent epifluorescence micrographs qualitatively validate our numerical simulation results and demonstrate steady state microfluidic mixing without visible instability along the contact interface. Another phenomenon visible in these micrographs (Figure 5e−h) is an increase in fluorescence intensity at the interface between the PBS and IPA streams. A likely cause of this phenomenon is an increase of the fluorescence yield of Sulforhodamine B (SRB) dye as a result of changes in microfluidic environmental polarity and viscosity as PBS mixes with IPA.[43] Figure 5 illustrates how Q_t modulates the convective−diffusive mixing of IPA with water in both the focusing region and the downstream mixing channel. In the numerical simulations, the contour and surface-to-volume ratio of the focused center stream change only minimally with Q_t, as a result of slightly different mixing and viscosity profiles. As shown in Figure 5, an increase in Q_t from 25 to 100 μL/min at a constant FRR of 14 or 49 in the 65 μm mixing channel device decreases the diffusive mixing between the focused IPA stream and sheathing water streams in the focusing region and spatially shifts the diffusive mixing process downstream. Additionally, at lower Q_t and hence lower *Pe*, the more viscous focused IPA stream may become progressively more ensheathed by the less viscous water stream, although this phenomenon is more relevant to systems with much larger viscosity contrasts.[42] To the extent that it occurs here, viscous ensheathing would increase the surface-to-volume ratio

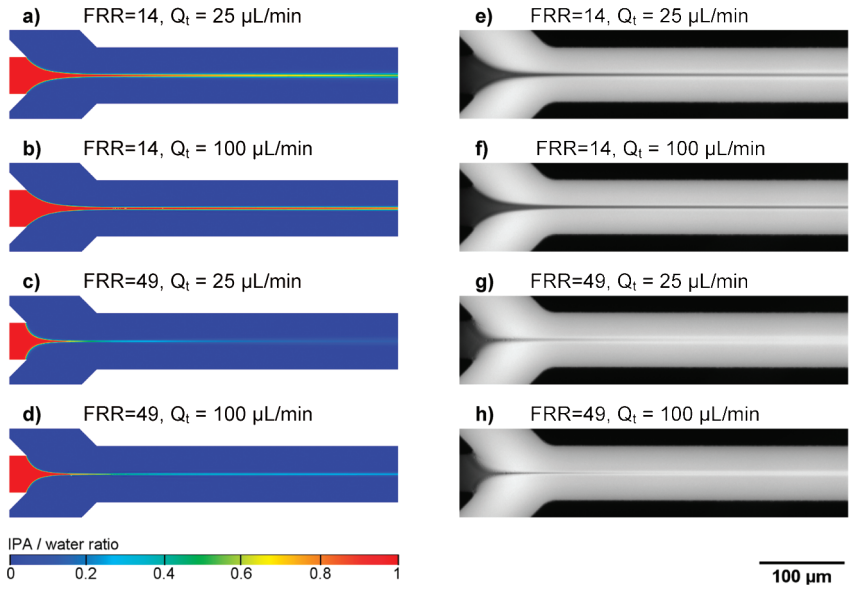

Figure 5. Numerical simulations of volumetric flow rate and hydrodynamic flow focusing. Simulated IPA concentration profiles of the focused stream at a low FRR of 14 (a, b) and high FRR of 49 (c, d) for a volumetric flow rate Q_t of 25 (a, c) and 100 µL/min (b, d) in the 65 µm wide channel geometry.

of the contact interface between the two liquids and result in faster mixing and smaller liposomes. Conversely, as Q_t and *Pe* increase, the process of ensheathing of IPA by water would become reduced or absent, which would reduce the surface-to-volume ratio of the contact interface between the two liquids and result in longer mixing times and larger liposomes. For both of these effects, an increasing fraction of lipid molecules self-assemble into larger liposomes in the diffusion-dominated mixing channel while the fraction of small liposomes formed in the convective-diffusive hydrodynamic focusing region decreases accordingly. Our experimental results in Figure 3 show that Q_t affects liposome size most significantly at low focusing conditions, while liposome size becomes independent of Q_t at high focusing conditions. Our corresponding simulations in Figure 5 show that the IPA concentration profile relevant to lipid solubility changes significantly over a large fraction of the microchannel length at a low FRR of 14, and as Q_t increases by a factor of 4 (Figure 5a,b) the peak liposome radius decreases by approximately 20 nm (Figure 3a). The IPA concentration above the solubility limit of lipid molecules changes only subtly at high FRRs (Figure 5c,d), resulting in minor changes in liposome size (Figure 3d). The effect of ensheathing would enhance mixing, particularly in the case of low Q_t, while ensheathing would decrease toward higher Q_t.

From our liposome synthesis experiments and numerical simulations of microfluidic mixing, we deduce that hydrodynamic focusing and total flow rate alter the relative amounts of liposome formation in the convective−diffusive hydrodynamic focusing region *versus* liposome formation in the diffusive mixing channel. Microfluidic device size and geometry set solid−liquid boundary conditions of the Navier−Stokes equations, which determine the hydrodynamic flow focusing profile and influence the relative amounts of rapid convective−diffusive mixing in the hydrodynamic focusing region and slow diffusive mixing in the downstream channel through the liquid−liquid interfaces. Figure 2 shows that as hydrodynamic focusing increases, liposome R_g converges toward a lower limit of about 22−25 nm for both channel geometries, and any noticeable reduction of R_g at FRR beyond 49 comes at the cost of diluting the sample. This lower liposome size limit at high FRRs and its invariance to Q_t suggest that all lipid molecules have self-assembled into liposomes within the convective−diffusive focusing region. An increase of Q_t at low focusing conditions increases the liposome radius, but the effects of Q_t diminish with increasing FRR. Modifying the flow focusing profile with FRR allows coarse-tuning of liposome size. At low focusing conditions Q_t provides a method to fine-tune the liposome size distribution, while at high focusing conditions, Q_t allows for an increase of throughput without changing liposome size.

Discussion of the Formation of Nanoscale Lipid Vesicles. The convective−diffusive mixing of alcohol and water, depletion of the focused alcohol stream through the fluidic interface, and separation of the vesicle formation process into different mixing domains provide a qualitative method to correlate vesicle size distributions with microfluidic mixing conditions. To interpret this correlation and connect it to existing theories of liposome assembly, we consider a well-known nonequilibrium model of vesicle formation which has been used to relate and explain a variety of disparate vesicle preparation systems.[44] This model is based on the formation of disk-like fragments or oblate micelles as an intermediate structure in the vesicle formation mechanism,

with final vesicle size depending not on equilibrium thermodynamics but instead on kinetic aspects of the formation process.[44−46] Within the structure of this theory, microfluidic mixing conditions producing smaller or larger liposomes correspond to the formation, growth, and closure of smaller or larger intermediate structures, respectively. A simple kinetic interpretation of our results is that a critical mixing time limits the growth of these nonequilibrium structures and forces vesicle closure.

Following this model, we infer several aspects of the microfluidic formation, growth, and closure of intermediate structures in the vesicle formation process. As a result of convective−diffusive mixing, lipid molecules initially dissolved in the focused IPA stream become exposed to an increasingly polar fluidic environment with decreasing lipid solubility. At a critical polarity, lipid molecules aggregate and form fragments or oblate micelles, and these intermediate structures grow through coalescence and/or the integration of solubilized lipid molecules.[44−46] One result of this growth process is a decrease in the diffusion coefficient of a lipid fragment and an increase in its tendency to advect along streamlines. As the polarity of the surrounding microfluidic environment continues to increase, these disk-like structures close and form vesicles to eliminate exposure of the lipid hydrocarbon tails.

To correlate the formation, growth, and closure of these intermediate structures with microfluidic mixing conditions, we consider the effects of hydrodynamic flow focusing and total flow rate. At low focusing conditions, only a small fraction of lipid molecules aggregates in the transition region close to the IPA/PBS interface, while a large fraction remains solubilized at higher IPA concentrations in the interior of the focused center stream. In the microchannel downstream of the focusing region, relatively slow diffusive mixing results in a gradual spatial and temporal concentration gradient. This mixing condition maintains lipid solubility for a longer duration and leads to a longer intermediate growth phase and larger liposomes. Since mixing is limited by diffusion under these conditions, volumetric flow rate provides a means to manipulate the formation and growth phase of fragments. As hydrodynamic focusing is increased, the critical mixing time transitions from a slower diffusion-limited mixing time to a faster convective-diffusive mixing time, and at high focusing conditions the intermediate growth phase is greatly limited by rapid convective-diffusive mixing. This abrupt spatial and temporal concentration gradient forces intermediate structures to rapidly form and close within the focusing region, resulting in small and narrow liposome size distributions.

To further investigate this process, we consider the advection of a lipid fragment or oblate micelle along different streamlines and kinetic concentration pathways for a given mixing condition. As follows from a combination of the IPA concentration simulation shown in Figure 4 and Figure 5 and corresponding fluid velocity simulations (not shown), an intermediate structure advecting along an outer streamline of the focused center stream experiences a rapid decrease in concentration caused by fast convective−diffusive mixing, which results in a shorter growth phase and a smaller liposome upon closure. Conversely, an intermediate structure closer to the interior of the focused center stream advects through a more gradual spatial and temporal concentration gradient with a longer diffusive growth phase, creating a larger liposome upon closure. These kinetic pathways are consistent with our correlation of liposome size to mixing region, as advection along inner and outer streamlines corresponds to diffusion-limited and convective-diffusive mixing and growth, respectively. These results also indicate a possible source of dispersity in liposome size distribution with COMMAND, which remains the subject of future work.

While our results are in qualitative agreement with an existing theory of nonequilibrium lipid vesicle formation, a quantitative elucidation of the liposome self-assembly process is confounded by a complex interplay of molecular and hydrodynamic phenomena, which is beyond the scope of this manuscript. Relevant phenomena include interactions between free lipid molecules and intermediate lipid structures in proximity, as well as the varying kinetic effects of diffusion and advection on these structures. Molecular and fluid dynamics simulations must be integrated in order to fully understand this process, which remains the subject of future work. Another approach which could be pursued in parallel is the application of a recently reported technique to image transient nanostructures using a combination of microfluidic mixing and cryogenic transmission electron microscopy.[47]

Another phenomena worth considering in the vesicle formation process as implemented is mechanical shear stress at the IPA−buffer interface in the focusing region. An increase in Q_t results in an increase of shear stress, and it might be expected that this would produce smaller liposomes, in a manner similar to the microfluidic formation of emulsions with immiscible fluids in which dispersed droplet size decreases with increasing shear stress.[48] In contradiction to this prediction, our results show that liposome size increases with Q_t and increasing shear forces at the miscible IPA−buffer interface. Furthermore, shear forces are restricted to the focusing region and cease as the focused stream enters the diffusive mixing channel. As focusing is decreased, however, an increasing fraction of liposome formation occurs in the mixing channel region and not the focusing region. Additionally, the shear forces in the focusing region of the 10 μm channel are significantly higher than those obtained in the 65 μm channel device for all total flow rates and flow rate ratios tested herein (results not shown) while similar lipo-

some size distributions are produced. These findings provide further evidence that shear forces play only a minor role in COMMAND and confirm that our approach is fundamentally different from microfluidic emulsification.

CONCLUSIONS

COMMAND enables the precise and predictable microfluidic mixing of miscible liquids under laminar flow, which provides a method for both on-chip liposome synthesis and the controlled experimental investigation of the self-assembly process of lipid molecules into nanoscale lipid vesicles. COMMAND confers the ability to reproducibly synthesize vesicle distributions with improved control over mean vesicle size and homogeneity, when compared to traditional bulk liquid phase liposome preparation techniques, while the continuous formation of nanoscale vesicles obviates bulk laboratory disassembly and assembly processes. In this manuscript, we studied COMMAND to develop a better understanding of the microfluidic environment that determines the liposome formation process and to facilitate further application of our technique. We found that microfluidic device design and fluid flow parameters act in concert to determine fluidic interfaces, convective-diffusive mixing, and liposome formation. As implemented, the formation of nanoscale lipid vesicles is an interfacial phenomenon, as bulk fluid flow parameters do not sufficiently describe the process. Different combinations of device geometry (*i.e.*, center inlet width, side channel width, outlet width, and length) and microfluidic parameters (FRR, Q_t) were used to produce similar liposome size distributions within the 50−150 nm size range. As such, for future liposome synthesis applications, microfluidic device design should be guided in large part by a desired technological advantage. To interpret our experimental results, we used numerical simulations of microfluidic mixing to develop the concept of a critical convective−diffusive mixing time which kinetically limits the growth and coalescence of lipid fragments. The combination of molecular and fluid dynamics simulations will play a critical role in the further elucidation of this process. We have also commenced preliminary investigations which indicate that the material properties of the alcohol−buffer system (*i.e.*, viscous anisotropy, polarity, ionic strength of the buffer) and the composition and concentration of the lipid blend also influence liposome size distribution, and are being investigated further. Finally, it is important to note that for many therapeutic applications of liposomes, it is desirable to remove alcohol residue from the final liposome formulation. This purification can be accomplished with dialysis, gel filtration chromatography, or through the further development of on-chip rinsing techniques for nanoscale vesicles.

MATERIALS AND METHODS

Note: Certain commercial materials and equipment are identified in order to adequately specify experimental procedures. In no case does such identification imply recommendation or endorsement by the National Institute of Standards and Technology, nor does it imply that the items identified are necessarily the best available for the purpose.

Device Fabrication. Microchannels were patterned and etched into the front side of a silicon wafer using standard photolithographic procedures and deep reactive-ion etching (DRIE). Aligned access holes were patterned and etched through the back side of the wafer by DRIE at each channel terminus, and the microchannels were sealed by anodic bonding of the silicon wafer to a borosilicate glass wafer. Two microchannel intersection layouts with different characteristic geometries and channel dimensions were designed and fabricated. The first design (Figure 1a) consists of a double-cross intersection in which the oblique side channels intersect with the corresponding end of the central channel at an angle of 45°. The channels have a rectangular cross section with a depth of 120 μm, a center inlet width of 42 μm, a mixing channel width of 65 μm, and a side channel width of 65 μm. The second design (Figure 1b) consists of two orthogonally intersecting microchannels with a rectangular cross section with a depth of 36 μm and a width of 10 μm. Nanoport fluidic connectors (Upchurch Scientific, Oak Harbor, WA) were adhered to the back sides of the silicon wafers to interface polyetheretherketone (PEEK) capillary tubing with the microchannel access points. Further details of device fabrication can be found elsewhere.[5]

Lipid Mixture and Hydration Buffer Preparation. Dimyristoylphosphatidylcholine (DMPC), cholesterol (Avanti Polar Lipids Inc., Alabaster, AL), and dihexadecyl phosphate (DCP) (Sigma-Aldrich) in a molar ratio of 5:4:1 were dissolved in chloroform (Mallinckrodt Baker Inc., Phillipsburg, NJ). The chloroform solvent was evaporated under a stream of nitrogen at room temperature to form a dry lipid film on the bottom of a glass scintillation vial, which was then placed into a vacuum desiccator for at least 24 h to ensure complete chloroform removal. The dried lipid blend was dissolved in isopropyl alcohol (IPA), a good solvent for cholesterol, at a 5 mmol/L total lipid concentration. Phosphate buffered saline (PBS) (Sigma Aldrich) solution (10 mmol/L phosphate, 2.7 mmol/L potassium chloride, 138 mmol/L sodium chloride, pH ≈ 7.4, 3 mmol/L sodium azide) was used as a hydration buffer.

Liposome Preparation. Unilamellar liposome samples were synthesized by injecting a lipid mixture dissolved in IPA from the left center channel of the microfluidic junctions shown in Figure 1a,b while injecting PBS into the two side channels intersecting with the center channel. Fluidic reagents were introduced into the center channel using a gastight glass syringe (Hamilton, Reno, NV) and into the side channels with plastic syringes (BD, Franklin Lakes, NJ) using syringe pumps (model PHD2000, Harvard Apparatus Inc., Holliston, MA). All fluids were filtered with 0.2 μm pore sized filters (Anatop, Whatman, NJ) to prevent particulate contamination and clogging of the microfluidic device. Liposomes were synthesized using the two microfluidic devices at varying buffer-to-lipid solution flow rate ratios (FRRs) and a constant average flow velocity (v_m) of 0.25 m/s in the mixing channel. The FRR, defined as the ratio of the buffer volumetric flow rate (Q_B) to the IPA volumetric flow rate (Q_S), was altered from 12 to 48 and from 6 to 36 in the 65 μm wide and 10 μm wide outlet channels, respectively. Liposome formation at different total volumetric flow rates (Q_t) of 25, 50, and 100 μL/min for differing FRRs of 14, 19, 29, and 49 was investigated in the 65 μm wide microchannel design. The liposome samples were collected from the outlet of the mixing channel in opaque centrifugation tubes (Argos, Elgin, IL) for subsequent analysis.

Light Scattering and Asymmetric Flow Field-Flow Fractionation (AF^4). High-resolution size-based separation of each liposome population was carried out using AF^4 with multiangle laser light scattering (MALLS) characterization (model DAWN EOS, Wyatt Technology, Santa Barbara, CA) as described previously.[5] PBS solution was used as a carrier liquid in the separations. A volume of 50 μL (sample volume from the 10 μm device) or 120 μL (sample volume from the 65 μm device) from the collected liposome sample was injected, and the radii of the eluted fractions of liposomes were monitored using the MALLS detectors. The MALLS intensity was measured at 12 angles simultaneously. A coated sphere model (*i.e.*, a spherical structure with two radial regions of differing refractive index) and a vesicle bilayer thickness of 4.5 nm were used to fit the light scattering data to estimate the geometric radius (R_g) of the fractionated samples.[49,50]

Numerical Simulation of Isopropyl Alcohol−Water Mixing Using Hydrodynamic Focusing. Concentration distributions of an injected IPA stream sheathed by two adjacent water streams were numerically simulated with a two-dimensional model using COMSOL Multiphysics 3.4 (COMSOL, Inc., Burlington, MA). Microfluidic flow and mixing dynamics are governed by the continuity and full Navier−Stokes equations for incompressible flow coupled to the convection−diffusion equation for the more viscous IPA fluid through a concentration-dependent viscosity. A single-phase fluid model was used throughout the numerical simulations with continuous shear stress and velocity across the contact interface and microchannel. The following set of equations were solved iteratively until steady-state was reached,

$$-\nabla\cdot\eta(\nabla\tilde{\mathbf{u}} + (\nabla\tilde{\mathbf{u}})^{\mathrm{T}}) + \rho(\tilde{\mathbf{u}}\cdot\nabla)\,\tilde{\mathbf{u}} + \nabla p = 0 \quad (1)$$

$$\nabla\cdot\tilde{\mathbf{u}} = 0 \quad (2)$$

$$-\nabla\cdot(-D\nabla c + c\tilde{\mathbf{u}}) = 0 \quad (3)$$

where η is the dynamic viscosity, $\tilde{\mathbf{u}}$ is the 2-D velocity vector, ρ is the density, p is the pressure, D is the mutual diffusivity, and c is the concentration of IPA. Equations 1−3 are subject to no-slip and no-penetration boundary conditions as well as zero diffusional flux at the wall,

$$\tilde{\mathbf{u}}(x_w) = 0 \quad (4)$$

$$\nabla c\cdot\hat{\mathbf{n}} = 0 \quad (5)$$

where x_w denotes the location of the wall and $\hat{\mathbf{n}}$ is the wall unit normal vector. The dynamic viscosity and mutual diffusion coefficient are a function of the IPA concentration and were expressed by a fourth order polynomial fitting empirical viscosity data and a second order polynomial fitting mutual diffusion coefficients as reported by Pratt *et al.*[32] In our simulations, the mixing of IPA with water was assumed to be homogeneous at the microscale, thereby neglecting microheterogeneities at the molecular scale due to alcohol cluster formation.[29,30,51] We also assumed a constant single-phase density, neglecting any possible diffusion-induced convection. Different values of FRR and v_m that correspond to experimental conditions were simulated for the 65 μm wide and 10 μm wide channels. Our simulations follow a similar approach to that described previously in several reports in which a two-phase fluid flow system is expressed as a single-phase system with concentration-dependent diffusion or viscosity.[52−55] While our simulations simplify the complex mixing process between alcohol and water, our aim is to make a qualitative comparison of different microfluidic mixing conditions.

Acknowledgment. This research was performed while S.M. Stavis held a National Research Council Research Associateship Award at the National Institute of Standards and Technology (NIST). Device fabrication was performed in part at the Cornell Nanoscale Science and Technology Facility (CNF), a member of the National Nanotechnology Infrastructure Network supported by the NSF, and in part at the NIST Center for Nanoscale Science and Technology (CNST). The authors thank the CNF and CNST staff for assistance with device fabrication and B. Nablo, J. Geist, J. Kralj, D. Ross, J. Zook, L.E. Locascio, and R. Tosh for critical review and helpful discussions.

REFERENCES AND NOTES

1. Bangham, A. D.; Standish, M. M.; Watkins, J. C. Diffusion of Univalent Ions across Lamellae of Swollen Phospholipids. *J. Mol. Biol.* **1965**, *13*, 238–252.
2. Lasic, D. D. Novel Applications of Liposomes. *Trends Biotechnol.* **1998**, *16*, 307–321.
3. Edwards, K. A.; Baeumner, A. J. Analysis of Liposomes. *Talanta* **2006**, *68*, 1432–1441.
4. Jahn, A.; Reiner, J. E.; Vreeland, W. N.; DeVoe, D. L.; Locascio, L. E.; Gaitan, M. Preparation of Nanoparticles by Continuous-Flow Microfluidics. *J. Nanopart. Res.* **2008**, *10*, 925–934.
5. Jahn, A.; Vreeland, W. N.; DeVoe, D. L.; Locascio, L. E.; Gaitan, M. Microfluidic Directed Formation of Liposomes of Controlled Size. *Langmuir* **2007**, *23*, 6289–6293.
6. Jahn, A.; Vreeland, W. N.; Gaitan, M.; Locascio, L. E. Controlled Vesicle Self-Assembly in Microfluidic Channels with Hydrodynamic Focusing. *J. Am. Chem. Soc.* **2004**, *126*, 2674–2675.
7. Knight, J. B.; Vishwanath, A.; Brody, J. P.; Austin, R. H. Hydrodynamic Focusing on a Silicon Chip: Mixing Nanoliters in Microseconds. *Phys. Rev. Lett.* **1998**, *80*, 3863–3866.
8. Meure, L. A.; Foster, N. R.; Dehghani, F. Conventional and Dense Gas Techniques for the Production of Liposomes: A Review. *AAPS PharmSciTech* **2008**, *9*, 798–809.
9. Wheeler, J. J.; Palmer, L.; Ossanlou, M.; MacLachlan, I.; Graham, R. W.; Zhang, Y. P.; Hope, M. J.; Scherrer, P.; Cullis, P. R. Stabilized Plasmid-Lipid Particles: Construction and Characterization. *Gene Ther.* **1999**, *6*, 271–281.
10. Hauschild, S.; Lipprandt, U.; Rumplecker, A.; Borchert, U.; Rank, A.; Schubert, R.; Forster, S. Direct Preparation and Loading of Lipid and Polymer Vesicles Using Inkjets. *Small* **2005**, *1*, 1177–1180.
11. Mayer, L. D.; Hope, M. J.; Cullis, P. R. Vesicles of Variable Sizes Produced by a Rapid Extrusion Procedure. *Biochim. Biophys. Acta* **1986**, *858*, 161–168.
12. Li, C. L.; Deng, Y. J. A Novel Method for the Preparation of Liposomes: Freeze Drying of Monophase Solutions. *J. Pharm. Sci.* **2004**, *93*, 1403–1414.
13. Wagner, A.; Vorauer-Uhl, K.; Kreismayr, G.; Katinger, H. The Crossflow Injection Technique: An Improvement of the Ethanol Injection Method. *J. Liposome Res.* **2002**, *12*, 259–270.
14. Gullotti, E.; Yeo, Y. Extracellularly Activated Nanocarriers: A New Paradigm of Tumor Targeted Drug Delivery. *Mol. Pharmaceutics* **2009**, *6*, 1041–1051.
15. Ishida, T.; Harashima, H.; Kiwada, H. Liposome Clearance. *Biosci. Rep.* **2002**, *22*, 197–224.
16. Hong, J. S.; Vreeland, W. N.; DePaoli Lacerda, S. H.; Locascio, L. E.; Gaitan, M.; Raghavan, S. R. Liposome-Templated Supramolecular Assembly of Responsive Alginate Nanogels. *Langmuir* **2008**, *24*, 4092–4096.
17. Kazakov, S.; Levon, K. Liposome−Nanogel Structures for Future Pharmaceutical Applications. *Curr. Pharm. Des.* **2006**, *12*, 4713–4728.
18. Schmidt, H. T.; Ostafin, A. E. Liposome Directed Growth of Calcium Phosphate Nanoshells. *Adv. Mater.* **2002**, *14*, 532–535.
19. Gomez-Hens, A.; Fernandez-Romero, J. M. The Role of Liposomes in Analytical Processes. *TrAC, Trends Anal. Chem.* **2005**, *24*, 9–19.
20. Reiner, J. E.; Jahn, A.; Stavis, S. M.; Culbertson, M. J.; Vreeland, W. N.; Burden, D. L.; Geist, J.; Gaitan, M. Accurate Optical Analysis of Single-Molecule Entrapment in Nanoscale Vesicles. *Anal. Chem.* **2010**, *82*, 180–188.
21. Karnik, R.; Gu, F.; Basto, P.; Cannizzaro, C.; Dean, L.; Kyei-Manu, W.; Langer, R.; Farokhzad, O. C. Microfluidic Platform for Controlled Synthesis of Polymeric Nanoparticles. *Nano Lett.* **2008**, *8*, 2906–2912.

22. Schabas, G.; Yusuf, H.; Moffitt, M. G.; Sinton, D. Controlled Self-Assembly of Quantum Dots and Block Copolymers in a Microfluidic Device. *Langmuir* **2008**, *24*, 637–643.
23. Johnson, S. M.; Bangham, A. D.; Hill, M. W.; Korn, E. D. Single Bilayer Liposomes. *Biochim. Biophys. Acta* **1971**, *233*, 820–826.
24. Macdonald, R. C.; Macdonald, R. I.; Menco, B. P. M.; Takeshita, K.; Subbarao, N. K.; Hu, L. R. Small-Volume Extrusion Apparatus for Preparation of Large, Unilamellar Vesicles. *Biochim. Biophys. Acta* **1991**, *1061*, 297–303.
25. Maulucci, G.; De Spirito, M.; Arcovito, G.; Boffi, F.; Castellano, A. C.; Briganti, G. Particle Size Distribution in DMPC Vesicles Solutions Undergoing Different Sonication Times. *Biophys. J.* **2005**, *88*, 3545–3550.
26. Ollivon, M.; Lesieur, S.; Grabielle-Madelmont, C.; Paternostre, M. Vesicle Reconstitution from Lipid-Detergent Mixed Micelles. *Biochim. Biophys. Acta, Biomembr.* **2000**, *1508*, 34–50.
27. Batzri, S.; Korn, E. D. Single Bilayer Liposomes Prepared without Sonication. *Biochim. Biophys. Acta* **1973**, *298*, 1015–1019.
28. Kremer, J. M. H.; Esker, M. W. J.; Pathmamanoharan, C.; Wiersema, P. H. Vesicles of Variable Diameter Prepared by a Modified Injection Method. *Biochemistry* **1977**, *16*, 3932–3935.
29. Dixit, S.; Crain, J.; Poon, W. C. K.; Finney, J. L.; Soper, A. K. Molecular Segregation Observed in a Concentrated Alcohol−Water Solution. *Nature* **2002**, *416*, 829–832.
30. Hawlicka, E.; Grabowski, R. Self-Diffusion in Water Alcohol Systems. 3. 1-Propanol Water Solutions of NaI. *J. Phys. Chem.* **1992**, *96*, 1554–1557.
31. Pratt, K. C.; Wakeham, W. A. Mutual Diffusion-Coefficient of Ethanol−Water Mixtures—Determination by a Rapid, New Method. *Proc. R. Soc. London, Ser. A* **1974**, *336*, 393–406.
32. Pratt, K. C.; Wakeham, W. A. Mutual Diffusion-Coefficient for Binary-Mixtures of Water and Isomers of Propanol. *Proc. R. Soc. London, Ser. A* **1975**, *342*, 401–419.
33. Engl, W.; Backov, R.; Panizza, P. Controlled Production of Emulsions and Particles by Milli- and Microfluidic Techniques. *Curr. Opin. Colloid Interface Sci.* **2008**, *13*, 206–216.
34. Shum, H. C.; Lee, D.; Yoon, I.; Kodger, T.; Weitz, D. A. Double-Emulsion Templated Monodisperse Phospholipid Vesicles. *Langmuir* **2008**, *24*, 7651–7653.
35. Brazhnik, K. P.; Vreeland, W. N.; Hutchison, J. B.; Kishore, R.; Wells, J.; Helmerson, K.; Locascio, L. E. Directed Growth of Pure Phosphatidylcholine Nanotubes in Microfluidic Channels. *Langmuir* **2005**, *21*, 10814–10817.
36. Dittrich, P. S.; Heule, M.; Renaud, P.; Manz, A. On-Chip Extrusion of Lipid Vesicles and Tubes through Microsized Apertures. *Lab Chip* **2006**, *6*, 488–493.
37. Funakoshi, K.; Suzuki, H.; Takeuchi, S. Formation of Giant Lipid Vesiclelike Compartments from a Planar Lipid Membrane by a Pulsed Jet Flow. *J. Am. Chem. Soc.* **2007**, *129*, 12608–12609.
38. West, J.; Manz, A.; Dittrich, P. S. Lipid Nanotubule Fabrication by Microfluidic Tweezing. *Langmuir* **2008**, *24*, 6754–6758.
39. Hertzog, D. E.; Michalet, X.; Jager, M.; Kong, X. X.; Santiago, J. G.; Weiss, S.; Bakajin, O. Femtomole Mixer for Microsecond Kinetic Studies of Protein Folding. *Anal. Chem.* **2004**, *76*, 7169–7178.
40. Brotherton, C. M.; Sun, A. C.; Davis, R. H. Computational Modeling and Comparison of Three Co-Laminar Microfluidic Mixing Techniques. *Microfluid. Nanofluid.* **2008**, *5*, 43–53.
41. Ismagilov, R. F.; Stroock, A. D.; Kenis, P. J. A.; Whitesides, G.; Stone, H. A. Experimental and Theoretical Scaling Laws for Transverse Diffusive Broadening in Two-Phase Laminar Flows in Microchannels. *Appl. Phys. Lett.* **2000**, *76*, 2376–2378.
42. Cubaud, T.; Mason, T. G. Formation of Miscible Fluid Microstructures by Hydrodynamic Focusing in Plane Geometries. *Phys. Rev. E: Stat., Nonlinear, Soft Matter Phys.* **2008**, *78*, 056308.
43. Magde, D.; Rojas, G. E.; Seybold, P. G. Solvent Dependence of the Fluorescence Lifetimes of Xanthene Dyes. *Photochem. Photobiol.* **1999**, *70*, 737–744.
44. Lasic, D. D. The Mechanism of Vesicle Formation. *Biochem. J.* **1988**, *256*, 1–11.
45. Antonietti, M.; Forster, S. Vesicles and Liposomes: A Self-Assembly Principle Beyond Lipids. *Adv. Mater.* **2003**, *15*, 1323–1333.
46. Leng, J.; Egelhaaf, S. U.; Cates, M. E. Kinetic Pathway of Spontaneous Vesicle Formation. *Europhys. Lett.* **2002**, *59*, 311–317.
47. Lee, J.; Jha, A. K.; Bose, A.; Tripathi, A. Imaging New Transient Nanostructures Using a Microfluidic Chip Integrated with a Controlled Environment Vitrification System for Cryogenic Transmission Electron Microscopy. *Langmuir* **2008**, *24*, 12738–12741.
48. Thorsen, T.; Roberts, R. W.; Arnold, F. H.; Quake, S. R. Dynamic Pattern Formation in a Vesicle-Generating Microfluidic Device. *Phys. Rev. Lett.* **2001**, *86*, 4163–4166.
49. Kerker, M. *The Scattering of Light, and Other Electromagnetic Radiation*; Academic Press: New York, 1969.
50. Korgel, B. A.; van Zanten, J. H.; Monbouquette, H. G. Vesicle Size Distributions Measured by Flow Field-Flow Fractionation Coupled with Multiangle Light Scattering. *Biophys. J.* **1998**, *74*, 3264–3272.
51. Wakisaka, A.; Ohki, T. Phase Separation of Water−Alcohol Binary Mixtures Induced by the Microheterogeneity. *Faraday Discuss.* **2005**, *129*, 231–245.
52. Sahu, K. C.; Ding, H.; Valluri, P.; Matar, O. K. Pressure-Driven Miscible Two-Fluid Channel Flow with Density Gradients. *Phys. Fluids* **2009**, *21*, 043603.
53. Sullivan, S. P.; Akpa, B. S.; Matthews, S. M.; Fisher, A. C.; Gladden, L. F.; Johns, M. L. Simulation of Miscible Diffusive Mixing in Microchannels. *Sens. Actuators, B* **2007**, *123*, 1142–1152.
54. Thangawng, A. L.; Howell, P. B.; Richards, J. J.; Erickson, J. S.; Ligler, F. S. A Simple Sheath-Flow Microfluidic Device for Micro/Nanomanufacturing: Fabrication of Hydrodynamically Shaped Polymer Fibers. *Lab Chip* **2009**, *9*, 3126–3130.
55. Wu, Z. G.; Nguyen, N. T. Hydrodynamic Focusing in Microchannels under Consideration of Diffusive Dispersion: Theories and Experiments. *Sens. Actuators, B* **2005**, *107*, 965–974.